Nanoscale

ARTICLE

Slow polymer diffusion on brush-patterned surfaces in aqueous solution

Received 00th January 2019,
Accepted 00th January 2019

DOI: 10.1039/x0xx00000x

www.rsc.org/

Christopher G. Clarkson,[a] Alexander Johnson,[b] Graham J. Leggett,[b] and Mark Geoghegan[a]*

A model system for the investigation of diffusional transport in compartmentalized nanosystems is described. Arrays of "corrals" enclosed within poly[oligo(ethylene glycol)methyl ether methacrylate] (POEGMA) "walls" were fabricated using double-exposure interferometric lithography to deprotect aminosilane films protected by a nitrophenyl group. In exposed regions, removal of the nitrophenyl group enabled attachment of an initiator for the atom-transfer radical polymerization of end-grafted POEGMA (brushes). Diffusion coefficients for poly(ethylene glycol) in these corrals were obtained by fluorescence correlation spectroscopy. Two modes of surface diffusion were observed: one which is similar to diffusion on the unpatterned surface and a very slow mode of surface diffusion that becomes increasingly important as confinement increases. Diffusion within the POEGMA brushes does not significantly contribute to the results.

Introduction

The two-dimensional diffusion of polymers in confined environments is of considerable current interest, given recent advances in measurement.[1, 2] The diffusion coefficients of polymers on uniform substrates exhibit different scaling laws with molar mass,[3, 4] raising new theoretical questions that are being addressed by computer simulations.[5, 6] Later work addressed gradient,[7] topographically-patterned,[8] and polymer-coated surfaces.[9] Additional aspects of polymer diffusion included "crowded" environments, where other polymers impede surface motion.[10, 11] Although crowded environments have substantial biological importance,[12, 13] the surface diffusion of biological macromolecules is also coupled to further confinement.

Compartmentalization is fundamental to the function of biological systems[14] and influences rates of diffusional transport.[15] For example, there is growing understanding of the role of crowding in controlling the kinetics of intracellular reactions.[16] Cell membrane function in particular involves a large number of efficient processes reliant on molecular diffusion.[17, 18] It has been suggested that the partitioning of the cell membrane enables a reliable control of diffusion.[19] In particular, the membrane-skeleton-fence and transmembrane-protein-picket (TPP) models describe how the proximity of the cell cytoskeleton to the membrane acts as a barrier to diffusion.[20-22] The barriers formed in the cell membrane serve to confine proteins and phospholipids to specific regions of the cell membrane for significant periods of time.[19]

In 1975, Saffman and Delbrück described the membrane as a thin layer of viscous fluid that is surrounded by a bulk liquid with very low viscosity.[23] Their model made it possible to use diffusion coefficients to infer the size of nanoscale objects like proteins. Later extensions allowed for the description of objects with any size,[24] and made possible the incorporation of micron-scale objects like domains of lipids. The Saffman-Delbrück (SD) model, also known as the 2D continuum-fluid model, treated the cell membrane as roughly homogeneous.

It was later observed that the behaviour of lipids in the membrane could not be caused by thermally induced Brownian motion as was predicted using the SD model.[22] Here, the lipid, 1,2-α-dioleoyl-*sn*-glycero-3-phosphoethanolamine (DOPE) experienced short term confinement followed by a long-term hopping between these areas of confinement. This process was referred to as hop diffusion. Within the compartment itself, diffusion of DOPE is comparable to that observed in liposomes. Further experiments have shown that this hop diffusion is a general behaviour.[20, 25-27]

The theory proposed to explain hop diffusion in the cell membrane was that the membrane skeleton acted in some way to partition the membrane. It is known from single molecule tracking that polymers on uniform surfaces in the presence of other polymers can exhibit rapid motion alternating with longer waiting times.[10] It is therefore useful to consider the movement of polymers confined to compartments but *without* the impediments caused by crowding.

The use of grafted polymers to delimit compartments is of considerable utility because of the ready control of geometrical and chemical parameters. These may be prepared using the self-assembly of microphase-separated block copolymers in a bottom-up approach,[28] or by lithography-based techniques.[29] It has been shown elsewhere that micrometre-scale arrays of

[a] *Department of Physics and Astronomy, University of Sheffield, S3 7RH, UK*
[b] *Department of Chemistry, University of Sheffield, S3 7HF, UK*
* *mark.geoghegan@sheffield.ac.uk*
Electronic Supplementary Information (ESI) available: See dx.doi.org/10.1039/x0xx00000x

end-grafted polymer "corrals" may be filled with supported lipid bilayers, or by polymer brush cushions that support lipid bilayers containing integral membrane proteins.[29, 30] This therefore seems to be a promising approach for investigating diffusion in confined systems, provided adequately small corrals can be produced. Approaches based on interferometric lithography (IL) are here shown to be appropriate for this problem.

Fluorescence correlation spectroscopy (FCS) is widely used for measuring diffusion coefficients, because it allows access to a broad range of time scales,[31-35] and can be operated on samples with complex microscale environments such as inside living cells.[1, 33, 36, 37] FCS uses a confocal experimental setup to achieve high spatial and temporal resolution. Unlike confocal microscopy, FCS requires a relatively low fluorophore concentration. This is because FCS is sensitive to fluctuations in fluorescence intensity and therefore depends upon few dye labels diffusing through the confocal volume for analysis. In general, the concentration of fluorescently tagged molecules should be of the order of 10 μmol m^{-3}, such that there is on average only one dye label within the detection volume at any given time. FCS has been established as an ideal tool for examining the diffusion of PEG on surfaces,[3, 7, 11, 38, 39] meaning that any deviations from normal behaviour will be clearly observed.

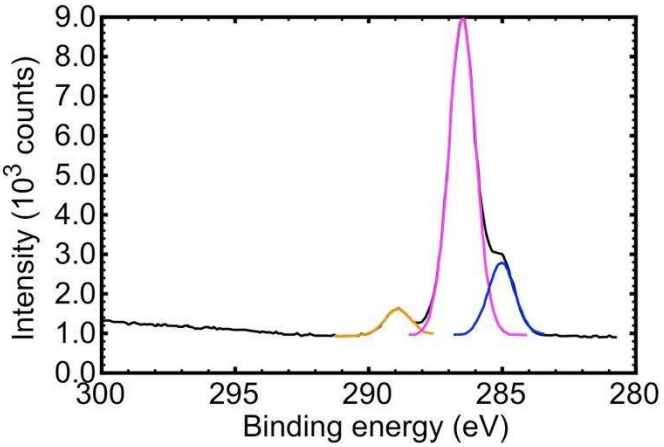

Fig. 1. C1s XPS spectrum for POEGMA contains three components in the peak envelope corresponding to the C–C/C–H (285.0 eV), C–O (286.4 eV) and COOR (288.8 eV) carbon atoms

Considerable research has been undertaken over many years to assess the impact that barriers have upon diffusion.[40-43] FCS can also be used to determine whether the cell membrane is formed of a meshwork or isolated microdomain structure:[44, 45] a methodology that has been applied in the current work

Here, a patterned polymer surface was used as an analogue of the structure of the cell membrane. The surface was partitioned into corrals where the only restriction on diffusion was the surface itself. The corrals were separated by a barrier of grafted polymers (brushes) created using IL, which hindered the surface diffusion. Because proteins interact non-specifically with a wide range of materials,[46-48] it is possible to simplify the problem further and replace them with poly(ethylene glycol) (PEG) as the molecule that diffuses on the surface. PEG is known to be inert in comparison to the biological molecules that are within the cell membrane. In fact, because PEG does not interact strongly with biological molecules,[49-52] it is often used as a coating to prevent proteins fouling surfaces.

To determine the effect of the barrier it is important that it be constructed so that it only behaves as a physical barrier, rather than producing a more complex interaction based on statics or strong nonpolar interactions. A simple solution is to use a barrier made of the very molecule that is diffusing. By tethering PEG to a substrate, a barrier can be constructed, with the PEG forming a polymer brush. To impart a dense barrier, the brush was made using poly[oligo(ethylene glycol)methyl ether methacrylate] (POEGMA). This polymer can be roughly treated as a methacrylate backbone surrounded by dense PEG chains.

Experimental

Growth of poly[oligo(ethylene glycol) methyl ether methacrylate) brushes

Materials. (3-aminopropyl)triethoxysilane (APTES) (99%), adipoyl chloride (98%) and glutaraldehyde (25% solution in H_2O) were supplied by Sigma-Aldrich (Poole UK). Ethanolamine was supplied by Riedel-de Haën. Sulfuric acid (1.83 S.G. 95+%), ammonium hydroxide solution (35%), hydrogen peroxide solution (30%) and ethanol (HPLC grade 99.8+%) were supplied by Fisher Scientific. Cover slips (22 mm × 64 mm and 22 mm × 26 mm, thickness 1.5 mm) were supplied by Menzel-Gläser. Oligo(ethylene glycol)methyl ether methacrylate (OEGMA, M_n = 475 g/mol), 2,2-bipyridyl (> 99%), copper(I) bromide (99%), copper(II) bromide (99%) were purchased from Sigma-Aldrich. 2-methacryloyloxy ethyl phosphorylcholine (MPC) was purchased from Lipidure. 2-nitrophenylpropyloxycarbonyl-protected (3-aminopropyl)triethoxysilane (NPPOC-APTES) was synthesised following a previously published method.[53]

Silane layer formation. To clean the glassware and substrates prior to the deposition of a silane layer, they were sonicated in a solution of sodium dodecyl sulfate (SDS) in water for 10 min and then rinsed with de-ionized (DI) water. The glassware and substrates were then immersed in piranha solution, a mixture of 30% hydrogen peroxide and 70% sulfuric acid, for 20-30 min before being rinsed and sonicated in DI water. (Considerable care was taken here because piranha solution can spontaneously detonate upon contact with organic material.) The substrates for silane layer formation were further cleaned in an RCA solution, which is a 5:1:1 mixture of H_2O:NH_4OH:H_2O_2, and heated to 80°C for 20 min before being rinsed thoroughly with DI water. To ensure the substrates and glassware were dry before use, they were placed in an oven at 120°C overnight. Films of APTES were prepared by immersing clean silicon or glass slides into a 1% (v/v) APTES solution in toluene for 30 min. After the formation of the monolayers, the slides were removed from solution, washed with toluene and ethanol and annealed in a vacuum oven at 120°C for 30 min. The monolayer films were then placed in a solution of 2.5 ml of dichloromethane (DCM), 10 L of triethylamine (TEA) and 3.5 L of 2-bromoisobutyryl

bromide (BiBB). The slides were left to react for 20-30 min and then rinsed with ethanol and DCM before being dried under a stream of nitrogen.

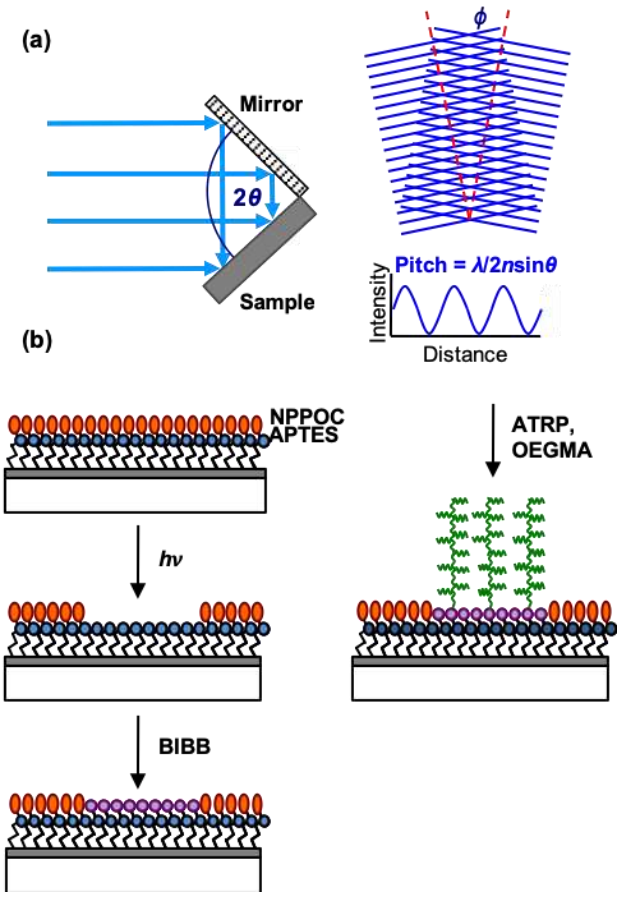

Fig. 2. (a) Schematic diagram of a Lloyd's mirror interferometer (left). Execution of a second exposure after rotation of the sample through an angle ϕ enables the fabrication of a grid pattern of exposure (right). (b) After exposure of NPPOC-APTES films, initiator is attached to exposed regions to enable spatially selected growth of polymer brushes

Surface-initiated ATRP reaction. In a round-bottom flask a mixture of 16 mL of DI water and 16.35 g of OEGMA was degassed with nitrogen for 30 min. To this solution 248 mg (1.58 mmol) of bipyridine (bipy), 80 mg (0.559 mmol) of Cu(I)Br, and 38 mg (0.17 mmol) of Cu(II)Br_2 were added. The solution was degassed for 5 min more and sonicated to dissolve any remaining solids. Slides of BIBB-APTES were then placed in a Schlenk tube, degassed and placed under nitrogen. The polymerization solution was carefully added to the Schlenk tubes to begin the atom-transfer radical polymerization (ATRP) process and left for 5-30 min depending on the brush height that was required. Once the polymerization step was complete the slides were removed and rinsed with methanol and sonicated in a 1:1 mixture of acetone and water before being dried under a stream of nitrogen.

Characterization of POEGMA brushes. The BIBB derivatized films, act as the ATRP initiator layer. Contact angle measurements were performed before and after the derivatization. The contact angle rose from 45° on the amine terminated surface to 69° when the BIBB group was present. This is in agreement with previous results.[54] The POEGMA brush, however, was completely hydrophilic and readily absorbed water.

X-ray Photoelectron Spectroscopy (XPS) was used to characterize the different surfaces. XPS was performed using a Kratos Axis Ultra spectrometer (Kratos Analytical, Manchester, UK) with a monochromatized Al Kα X-ray source operating at 150 W with an emission current of 8 mA and a pressure in the analysis chamber of between 10^{-8} to 10^{-10} mbar. Electron energy analyser pass energies of 160 eV and 20 eV were used to acquire survey (wide) scans and high-resolution spectra, respectively. The samples were prepared with approximate dimensions of 5×5 mm^2 and then rinsed with ethanol and dried under dry N_2 before analysis. High-resolution peaks were fitted and processed using CasaXPS software (Casa Software Ltd, Teignmouth, UK). In the XPS spectrum a Br 3d peak was observed at 68.9 eV while in the C 1s spectrum of the BIBB-APTES surface three components were fitted to the peak. These components indicate the presence of C–H/C–C (285.0eV), C–Br/C–NCO carbons (286.4eV) and O=CN (288.0eV) carbon atoms. The POEGMA surface was similarly characterized (**Fig. 1**).

Patterned polymer brush surfaces

Patterned surfaces were fabricated by using IL. Exposure of NPPOC-APTES to an interferogram formed using a Lloyd's mirror interferometer in conjunction with a Coherent Innova 300C frequency-doubled argon ion laser emitting at 244 nm caused selective removal of the NPPOC protecting group. For the work described here, a double-exposure process was used, in which the sample was rotated through 90° between exposures. Deprotected regions of the sample were derivatised with Br initiators for ATRP by reaction with BiBB.

Fluorescence correlation spectroscopy

A Carl Zeiss Axiovert 200M microscope with an inverted stage connected to an FCS (ConfoCor2) module was used for all FCS measurements, which were performed in an air-conditioned room at 18°C. The objective used was a C-Apochromat water immersion lens with a magnification of 40 $\times$ and a numerical aperture of 1.2. A HeNe laser was used to excite the sample at 543 nm. An HFT 543 dichroic beamsplitter was used. A BP 560-615 band pass filter was used to select only photons with wavelengths between 560 nm and 615 nm to be counted. The FCS is equipped with a neutral density filter to limit photobleaching, but the laser power was kept low enough so the signal remained constant. The fluorescent tag used was Rhodamine B (RhB), which has an absorption peak at 540 nm and an emission peak at 565 nm. The RhB was pre-attached to one end of poly(ethylene glycol) with a methyl group at the other end (mass average molar mass, M_w of 1, 5, 20 and 40 kDa and dispersities less than 1.10 as stated by the manufacturer) and purchased from Nanocs (New York) and used as supplied. RhB used for calibration was purchased from Sigma-Aldrich for calibration purposes. Coverslips were obtained from Fisher-Scientific.

Calibration. The set-up was calibrated using a solution of free RhB. A solution of RhB in milliQ water was diluted to 10^{-8} mol L^{-1} and 1 mL was placed on a coverslip within a silicone isolator. A second

coverslip was then mounted onto the isolator. 100 µL of milliQ water was then placed on the objective lens and the coverslip was placed into the standard microscope mounting. A diffusion measurement was taken for 6 s and repeated 100 times. The resulting autocorrelation data were averaged and then fitted to obtain a diffusion time for RhB through the confocal volume. The diffusion coefficient of RhB in water is (427 ± 4) µm^{2}s^{-1} at 298.15 K.[55, 56] This diffusion coefficient is substantially greater than the diffusion of the rhodamine-labelled polymer in solution, and so it was possible to confirm the absence of loose dye in the solution.

Surface diffusion. The concentration of dye molecules was tuned to 10^{-8} mol L^{-1} and 100 L of the solution placed upon the objective lens. The surface was located by a optimizing a height scan to maximize intensity. For each surface, measurements of each polymer were taken consecutively. Measurements of 3 s were repeated 100 times for a total acquisition time of 5 min. Data were fitted to the autocorrelation function,

$$G(\ ) = \frac{G_3(\ )}{n}\left(\frac{1}{\left(1+\left(\frac{\ }{\ _1}\right)^2\right)\sqrt{1+\frac{\ }{\ _1 S^2}}} + \frac{f_2}{1+\frac{\ }{\ _2}} + \frac{f_3}{1+\frac{\ }{\ _3}}\right) \quad (1)$$

using a Levenberg-Marquardt algorithm in the software ProFit 6 (QuantumSoft, Switzerland) as described previously.[7] The diffusion times in both two (τ_2 and τ_3) and three dimensions (τ_1) was extracted from these data, along with the fractional surface coverages (f_2 and f_3) and the number of molecules in the confocal volume, n. The subscripts 2 and 3 indicate two discrete surface diffusion components. The parameter S^2 is a pre-calibrated instrumental parameter describing the shape of the confocal volume and $G_3(\tau)$ is the autocorrelation function for the triplet decay. A good optimization of the surface intensity generally resulted in a very small contribution from bulk (i.e. three-dimensional) diffusion. The error associated with each diffusion time is related to the standard error from the fitting of the correlation curves and the uncertainty from the determination of the FCS beam size. The error associated with the proportion of each component is the standard error from the fitting of the raw correlation curves. It is possible for the FCS to detect asymmetry in the surface diffusion,[7] but such effects were not observed in this work and **eqn (1)** was always suitable for fitting the data.

Results and discussion

Fabrication of arrays of wells

The process used to fabricate arrays of sub-micrometre scale wells is shown schematically in **Fig. 2**. A Lloyd's mirror interferometer was used to pattern films formed by the adsorption of 2-nitrophenylpropyloxycarbonyl-protected (3-aminopropyl)triethoxysilane (NPPOC-APTES) on glass substrates (**Fig 2a**). The interferogram consisted of alternating bands of constructive and destructive interference (high and low intensity, respectively) with a pitch of $\lambda/2\sin\theta$, where λ is the wavelength used and 2θ is the angle between the interfering beams of light. In regions that were exposed to maxima in the interferogram, the NPPOC protecting group was removed, exposing the amine group of APTES and enabling subsequent derivatization by reaction with BiBB. Polymer nanostructures were grown by ATRP from the resulting initiator nanopatterns.

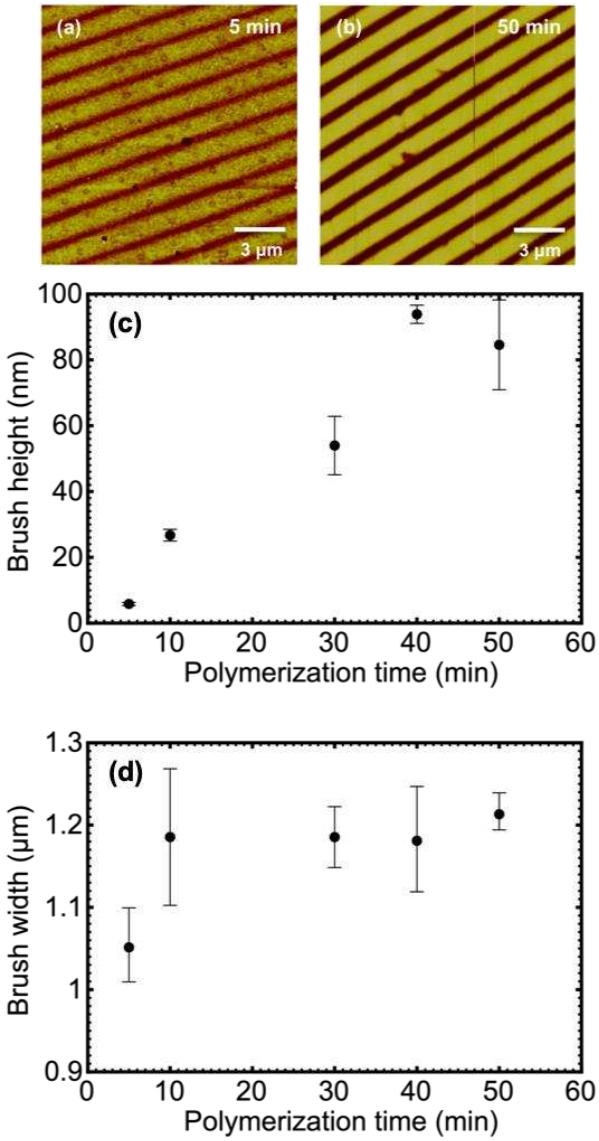

Fig. 3. (a,b) Scanning force microscopy topographical images of two sets of POEGMA nanostructures formed using IL in combination with ATRP. The polymerization times used were different (5 and 50 min), but all other conditions were identical for the same samples. (c,d) Variation in the polymer feature width and height, respectively, as a function of the polymerization time for a fixed set of exposure conditions in the interferometer

The dimensions of the nanostructures were adjusted by varying the UV dose (the larger the dose the greater the width of the deprotected region); the angle between the interfering beams of light (which causes a change in the pitch of the interferogram); and the polymerization time. **Fig. 3a,b** shows scanning force microscopy images of POEGMA nanostructures formed with a pitch of ~1.7 µm. The exposure conditions in the

interferometer were identical but the polymerization time was varied. On visual inspection, the pitch of the structures and the widths of the polymer regions appear to be similar. **Fig. 3d** shows the widths of the polymer nanostructures as a function of the polymerization time. It can be seen that there is little change for polymerization times of 10 min and greater. However, the polymer height (measured from line sections through topographical images) increases monotonically as a function of the polymerization time (**Fig. 3c**), confirming that in these nanostructured materials ATRP is well controlled.

A double exposure process was used to make arrays of wells. The sample was rotated through an angle of 90° between exposures for all of the samples used in the present study. After derivatization with Br initiators and ATRP a pattern of intersecting lines of polymer was produced, thus creating a grid of approximately square polymer-free regions in which the NPPOC protecting groups remained intact at the surface. **Fig. 4** shows three different arrays of wells, formed with periods of 760 nm, 400 nm and 200 nm. It is clear that the wells are well-defined in all cases. The well size is typically ~45% of the period in the interferogram. Well sizes in the range 100 – 600 nm were used in the present study. The surfaces created for this work are tabulated in the **ESI**.

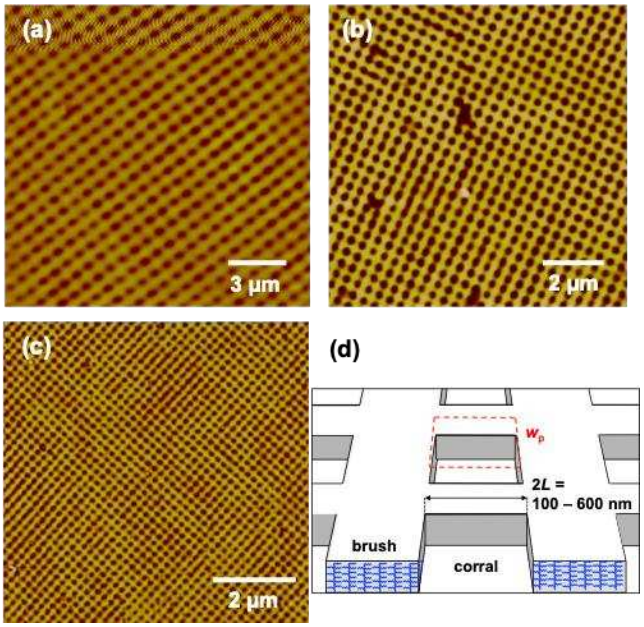

Fig. 4. (a-c) Arrays of wells formed by using interferometric lithography in combination with ATRP of POEGMA. (d) Schematic diagram showing the dimensions of the well structures and the parameters used to describe them

Diffusion coefficients

Control measurements demonstrate that the PEG diffused on unmodified NPPOC-APTES films at between 6 and 8 $\mu m^2 s^{-1}$, depending upon the molar mass of the polymer used. The diffusion coefficient of 20 kDa rhodamine 6G-terminated PEG on gold was measured[9] to be 11.7 $\mu m^2 s^{-1}$ which is in good agreement given the water contact angle of gold[57, 58] of ~70° is the same as that measured on NPPOC as part of this study, and which is also in agreement with earlier work.[53] Given that rhodamine B is a relatively hydrophilic dye,[59] it is also unlikely that it is causing any unwanted adhesive interactions with these surfaces.

By contrast, the diffusion of PEG in the POEGMA brush was seen to proceed with a diffusion coefficient of between 15 and 20 $\mu m^2 s^{-1}$, again dependent upon the molar mass of the PEG. It is known that PEG does not (measurably) diffuse on PEG surfaces[60] but that diffusion within the brush is possible. Experiments have shown that 20 kDa PEG diffuses within 20 kDa brushes with diffusion coefficients of between 1.1 and 9.5 $\mu m^2 s^{-1}$ depending on the grafting density.[9] This informs the conclusion that the PEG here is diffusing *in* rather than *on* the POEGMA surface.

Quantifying the diffusion of PEG on IL-patterned surfaces is non-trivial because of the two-component structure of the surface. Had the brush component been negligibly narrow, then the area of the patterns, or the associated length scale would be sufficient. However, in this case the brush layer has a finite volume. The length of the internal perimeter of the brush structures, w_p, provides one means to quantify the change in morphology of the patterned brush structure. In addition, the focal diameter, W, from the FCS experiments can be related to the width of the well, $2L$ (**Fig. 4d**), to yield a confinement parameter, X_c^2, defined by[45]

$$X_c^2 = \frac{W^2}{4L^2}. \qquad (2)$$

The confinement parameter was designed to address the problem that the number of structures contained within the focal area is ill-defined, due to an imprecise location of the confocal volume. By varying W, some control over confinement could be obtained, allowing different models to be tested. In the present case, L was varied. The errors associated with the confinement parameter are a combination of the uncertainty in the measurement of the size of the polymeric grids and the standard error obtained when determining the size of the FCS beam waist.

In the case of these patterned surfaces, three diffusion modes were observed. These corresponded to diffusion in the bulk, on the surface, and a third very slow surface diffusion mode was also observed in all samples and across all molar masses of PEG. **Fig. 5** shows normalised correlation curves obtained from the diffusion of 1 kDa PEG on the patterned surfaces and all of the diffusion coefficients corresponding to these confined systems are plotted as a function of confinement parameter in **Fig. 6**. The validity of adding the third diffusion mode (second surface mode) was confirmed through the use of a statistical F-test. The bulk diffusion is unaffected by the increase in confinement parameter, primarily with the same proportion of molecules diffusing independently of confinement parameter. The first, faster surface diffusion mode, appears to relate to a consistent diffusion time across the range of confinement parameters. The slower surface mode becomes more prominent with an increase in the confinement parameter, yet the diffusion times also remain constant across the range observed. The ratio describing the proportions of the fast and slow diffusion modes changes with confinement parameter, with the slower mode becoming more prominent with increasing X_c^2 (**Fig. 7**).

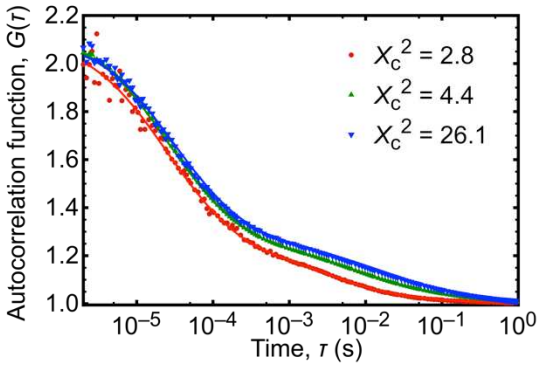

Fig. 5. Normalized correlation curves and fits to **eqn (1)** showing the diffusion of 1 kDa PEG chains on three different patterned polymeric grid surfaces, with respect to the confinement parameter that defines each surface. The curves show both the diffusion of PEG in the water above the surface and diffusion upon it. The bulk component is unaffected by the differing patterns upon the surface, with the introduction of a second mode of diffusion, whose proportion increases as the confinement parameter increases. This can be seen as an overall slowing of diffusion as the well size decreases

Once the raw curves were fitted it was possible to extract information such as the diffusion times of each mode and the proportion of molecules associated with each mode. Molecules from each regime were not necessarily fixed in their behaviour; for example, molecules in the bulk may adsorb on the surface and then spend some time in either of the two surface modes, perhaps even transforming between the two, before returning to the bulk.

Fig. 6 shows fitted values for the diffusion coefficients for the four PEG samples, with the 1 kDa data highlighted in **Fig. 6a** to show error bars. The bulk data are consistent with previously published results.[3, 38] The fast mode is essentially the same as that for diffusion on the NPPOC-terminated surface. The diffusion coefficient is dependent on molar mass but there is no dependence on the degree of confinement. The slow surface diffusion is similar in magnitude to that of the diffusion of single tracer molecules through a polymer brush,[61] but polymer diffusion within the brush is rather similar to that in the equivalent semi-dilute solution[9] and is not retarded. However, the slow diffusion indicates that the polymer is interacting with the barriers that these brushes present.

Confinement

The proportions of molecules exhibiting each mode of diffusion changes with increasing X_c^2 within the range observed as shown in **Fig. 5**. As X_c^2 increases, the proportion of molecules exhibiting the slow surface diffusion mode increases until a threshold is met, above which it is independent of X_c^2. This threshold is met for smaller X_c^2 for larger PEG, and also the fraction of molecules at this threshold increases with molar mass, although the two largest PEG samples studied have the same concentration at threshold (~40%). The fraction of molecules on the surface diffusing in this slow mode was fitted with an empirical function given by

$$f = \frac{A}{2}\left(1+\mathrm{erf}\left(BX_c^2 \quad C\right)\right) \qquad (3)$$

where A, B, and C are fitting parameters. These fits are generally very good and are shown in **Fig. 7a**, and the results obtained are included in the **ESI**. For small values of X_c^2 the fitted parameters indicate that there would be a significant non-zero fraction of molecules undergoing diffusion in the slow surface mode on non-patterned, homogeneous NPPOC-protected surfaces. This was not observed in experiments on these surfaces. It was not possible to obtain good fits by forcing $f(X_c^2 = 0) = 0$.

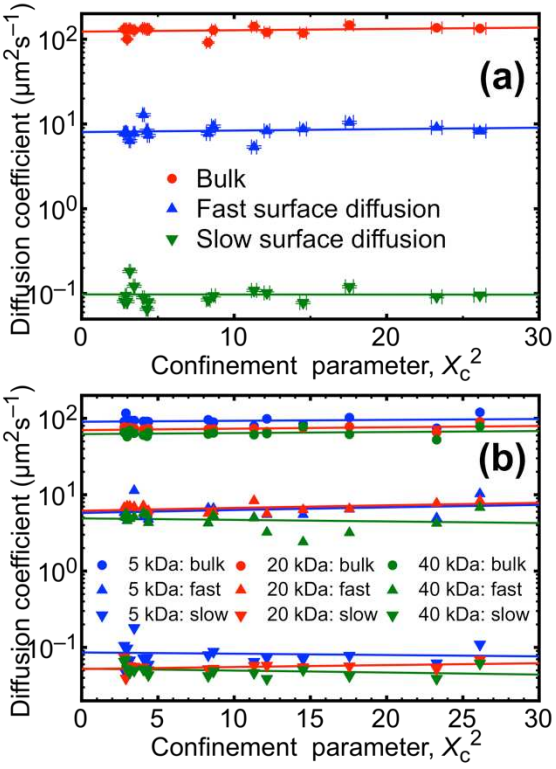

Fig. 6. (a) Diffusion coefficients of 1 kDa PEG molecules on a patterned polymeric grid surface plotted with respect to the confinement parameter X_c^2. Three separate diffusion coefficients are observed, corresponding to three modes of diffusion. Errors in diffusion coefficient are plotted but are very small in comparison to the size of their marker. (b) As in (a), but for the other three polymers used in this study. Here error bars are not shown. The bulk diffusion coefficients extracted from these data for the different PEG samples in order of increasing molar mass are: 123 ± 4, 93 ± 3, 73.1 ± 1.5, and 64 ± 2 μm²/s

In **Fig. 7b** the proportion of PEG diffusing in the slow mode is shown as a function of well perimeter observable within the FCS confocal area. The value for this parameter is reached by treating each well as a discrete point on a square lattice, and then applying the logic used in the solution to the Gauss circle problem to get an average number of wells and an associated uncertainty. Formally, the Gauss circle problem is appropriate when there is a large number of lattice points, but the solution provided here still gives a good estimate for the amount of interface that will be present. These curves are sharper than those plotted as a function of X_c^2, which indicates that the transition from normal to confined motion can be considered due to the amount of interface. (The significance of $w_p \approx 0.7$ μm as the transition point is not clear, however.) Furthermore, fits to **eqn (3)** pass through the origin, which is not shown in **Fig. 7b**. The curves are also more clustered because the confinement transition is localized around the same point, although the width of this transition increases with molar mass.

There has been very little work describing the effect of nanoconfinement on surface diffusion, although topographically-structured surfaces have been shown to influence surface diffusion,

with larger structures (greater confinement) introducing subdiffusive behaviour.[8]

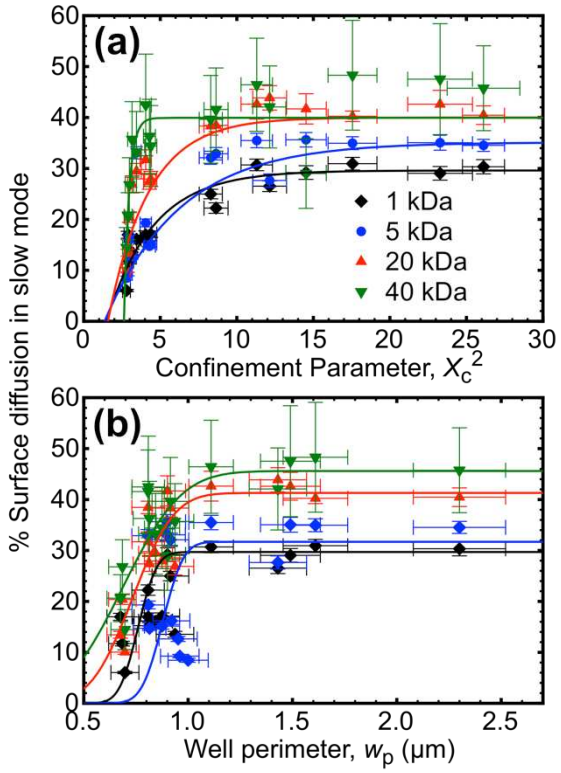

Fig. 7. The percentage of surface diffusion of PEG that is in the slow surface diffusion mode presented in terms of (a) the confinement parameter and (b) well perimeter. Solid lines are fits to **eqn (3)**

Microdomains

It has been shown from FCS measurements at different spatial scales that different models of confinement could be distinguished.[45] These models are significant because, on short timescales, the polymer undergoes Brownian motion. However, on longer timescales it interacts with the surrounding walls, which confine the polymer and limit its diffusion. On long timescales the polymer can escape the well in which it was confined, and so the diffusional behaviour can be considered to be similar to Brownian motion, although it occurred as a sequence of hops. Confinement can also act as a proxy for timescales. The more confined the structure is, the shorter the time at which the polymer takes to hop from one structure to another. The average (surface) diffusion time ($\tau_a = f\tau_2 + (1-f)\tau_3$) plotted as a function of confinement parameter can be used to reveal information on how the polymer interacts with the structure confining it. These plots are shown in **Fig. 8** and, following previous work,[45] two regions have been delimited for $2 < X_c^2 < 10$ and $X_c^2 > 10$. In the former case, the intercept of the extrapolated data is with a negative τ_a, which indicates that the polymer is trapped in a mesh structure. For the latter more confined case, the diffusing polymer experiences a series of isolated microdomains.

When $X_c^2 > 2$, the laser spot is larger than the patterned structure. The confinement parameter here is a proxy for the beam spot area, and if this were to be extrapolated to the origin the diffusion would be expected to be Brownian. The negative intercept shown for $2 < X_c^2 < 10$ reflects the significant effect of the barriers in the diffusion process; increasing X_c^2 is akin to decreasing the time required for the polymer to hop out of one structure and into another. The negative intercept therefore reflects the fact that a polymer may take p_1 steps to reach a distance of d_1, representing the edge of the structure. If that distance d is decreased to d_2, the number of steps to reach the edge, $p_2 < p_1(d_2/d_1)^2$ because the polymer is proportionally more likely to be closer to the edge of the structure to begin with in a more confined system.

For heavily confined systems, the effect of confinement is determined more by the time taken to hop from one structure to another than by the simple step time. In this case, a positive τ_a intercept is observed.

Partition confinement

In the work described here, the PEG was not retained within the structures and was free to diffuse into the surrounding solution, which is contrary to the case of biological systems whereby virtually all molecules remain within the confining structure. Nevertheless, the slow surface mode was brought about by an interaction with the brush and is perhaps more closely linked with the mechanism that causes hop diffusion in the cell membrane. The PEG 'hops' from well to well with some interaction confining polymers to a well for a certain period.

In the cell membrane, almost all membrane molecules are confined by the partitions. Larger molecules are affected more strongly, but even lipids are affected, with the vast majority of lipids exhibiting noticeably slower diffusion coefficients than in artificial membranes.[62-70] In the present work, a maximum of 45% of surface diffusion is in the slower mode (as taken from fitted values of 40 kDa PEG treated in terms of well perimeter). This is a significant proportion of polymers undergoing surface diffusion in the corrals. It has been suggested elsewhere[21, 71-73] that protein-protein and protein-lipid interactions primarily lead to the partitioning behaviour. It was shown here that confined behaviour (through a new slow diffusion mode) can be produced without the need for these more complex interactions. This does not imply that protein-protein and protein-lipid interactions are not important in diffusion within the cell membrane. Simply having a nanoscale structure induces anomalous diffusion behaviour.

Conclusions

The surface diffusion of PEG within POEGMA confining walls has been shown to introduce a slow surface mode that is unconnected with either of the individual surfaces from which the structure is composed. FCS measurements of the diffusion reveal three modes of PEG diffusion, comprising a bulk diffusion, a diffusion on the interior (NPPOC-protected) surface of the patterned structures, and a slow confined diffusion that appears to result from the pattern constraining the PEG. This slow diffusion represents confined behaviour and is solely a structural parameter. The POEGMA brush confining structure and the NPPOC-coated surface contain no specific interactions

such as those involved in the cell membrane, but still have a significant effect polymer motion.

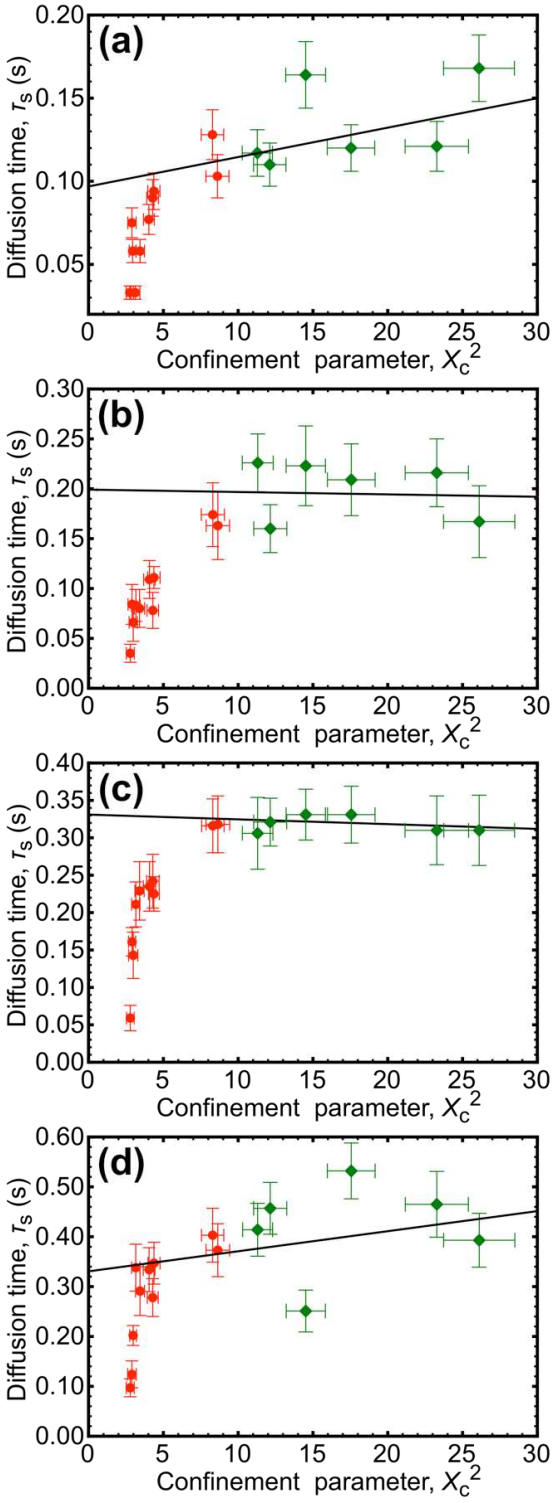

Fig. 8. The diffusion time as a function of the confinement parameter. When $X_c^2 > 2$, the laser spot is larger than the patterned structure and the data are presented as green diamonds. The black lines are fits to the data for $X_c^2 > 10$. The data correspond to diffusing PEG with molar mass 1 kDa (a), 5 kDa (b), 20 kDa (c), and 40 kDa (d)

Furthermore, the work shows how using methods developed for cell biology studies, some understanding of synthetic structures can be obtained. FCS is limited by the size of its beam, but by varying the size of the structure created using interferometric lithography some understanding of the diffusion of PEG within these structures was obtained, and also some understanding of the structures themselves as experienced by the diffusing molecule. In the present work, it is shown that heavily confined structures are presented as similar to isolated microdomains, whereas less confined architectures are considered an ordered mesh-like structure.

Conflicts of interest

There are no conflicts of interest to declare.

Acknowledgements

We gratefully acknowledge financial support from the Engineering and Physical Sciences Research Council under Programme grant EPSRC EP/I012060/1.

Electronic supplementary information

Further FCS data to complement **Fig. 5**; data showing the parameters describing the different surfaces, and a table of lipid diffusion coefficients.

Notes and references

1. M. Mears, D. S. Tarmey and M. Geoghegan, *Macromol. Rapid Commun.*, 2011, **32**, 1411-1418.
2. H. Miller, Z. Zhou, J. Shepherd, A. J. M. Wollman and M. C. Leake, *Rep. Prog. Phys.*, 2018, **81**, 024601.
3. S. A. Sukhishvili, Y. Chen, J. D. Müller, E. Gratton, K. S. Schweizer and S. Granick, *Macromolecules*, 2002, **35**, 1776-1784.
4. J. S. S. Wong, L. A. Hong, S. C. Bae and S. Granick, *Macromolecules*, 2011, **44**, 3073-3076.
5. T. G. Desai, P. Keblinski and A. Kumar, *J. Chem. Phys.*, 2008, **128**, 044903.
6. H.-J. Qian, L.-J. Chen, Z.-Y. Lu and Z.-S. Li, *Phys. Rev. Lett.*, 2007, **99**, 068301.
7. P. Burgos, Z. Zhang, R. Golestanian, G. J. Leggett and M. Geoghegan, *ACS Nano*, 2009, **3**, 3235-3243.
8. D. Wang, C. He, M. P. Stoykovich and D. K. Schwartz, *ACS Nano*, 2015, **9**, 1656-1664.
9. Z. J. Zhang, S. Edmondson, M. Mears, J. Madsen, S. P. Armes, G. J. Leggett and M. Geoghegan, *Macromolecules*, 2018, **51**, 6312-6317.
10. G. T. Morrin and D. K. Schwartz, *Macromolecules*, 2018, **51**, 1207-1214.
11. J. Zhao and S. Granick, *Macromolecules*, 2007, **40**, 1243-1247.
12. M. R. Horton, F. Höfling, J. O. Rädler and T. Franosch, *Soft Matter*, 2010, **6**, 2648-2656.
13. I. Munguira, I. Casuso, H. Takahashi, F. Rico, A. Miyagi, M. Chami and S. Scheuring, *ACS Nano*, 2016, **10**, 2584-2590.
14. B. Liu, C. Åberg, F. J. van Eerden, S. J. Marrink, B. Poolman and A. J. Boersma, *Biophys. J.*, 2017, **112**, 1929-1939.
15. P. E. Schavemaker, W. M. Smigiel and B. Poolman, *eLife*, 2017, **6**, e30084.

16. F. Bianchi, Ł. Syga, G. Moiset, D. Spakman, P. E. Schavemaker, C. M. Punter, A.-B. Seinen, A. M. van Oijen, A. Robinson and B. Poolman, *Nature Commun.*, 2018, **9**, 501.
17. M. Şener, J. Strümpfer, J. A. Timney, A. Freiberg, C. N. Hunter and K. Schulten, *Biophys. J.*, 2010, **99**, 67-75.
18. M. K. Şener, J. D. Olsen, C. N. Hunter and K. Schulten, *Proc. Natl Acad. Sci. USA*, 2007, **104**, 15723-15728.
19. A. Kusumi, C. Nakada, K. Ritchie, K. Murase, K. Suzuki, H. Murakoshi, R. S. Kasai, J. Kondo and T. Fujiwara, *Annu. Rev. Biophys. Biomol. Struct.*, 2005, **34**, 351-378.
20. K. Murase, T. Fujiwara, Y. Umemura, K. Suzuki, R. Iino, H. Yamashita, M. Saito, H. Murakoshi, K. Ritchie and A. Kusumi, *Biophys. J.*, 2004, **86**, 4075-4093.
21. R. Iino, I. Koyama and A. Kusumi, *Biophys. J.*, 2001, **80**, 2667-2677.
22. T. Fujiwara, K. Ritchie, H. Murakoshi, K. Jacobson and A. Kusumi, *J. Cell Biol.*, 2002, **157**, 1071-1081.
23. P. G. Saffman and M. Delbrück, *Proc. Natl Acad. Sci. USA*, 1975, **72**, 3111-3113.
24. B. D. Hughes, B. A. Pailthorpe and L. R. White, *J. Fluid Mech.*, 1981, **110**, 349-372.
25. Y. Sako and A. Kusumi, *J. Cell Biol.*, 1994, **125**, 1251-1264.
26. Y. Sako, A. Nagafuchi, S. Tsukita, M. Takeichi and A. Kusumi, *J. Cell Biol.*, 1998, **140**, 1227-1240.
27. M. Tomishige, Y. Sako and A. Kusumi, *J. Cell Biol.*, 1998, **142**, 989-1000.
28. E. Chu, T. Babar, M. F. Bruist and A. Sidorenko, *ACS Appl. Mater. Interfaces*, 2015, **7**, 12505-12515.
29. A. Johnson, J. Madsen, P. Chapman, A. Alswieleh, O. Al-Jaf, P. Bao, C. R. Hurley, M. L. Cartron, S. D. Evans, J. K. Hobbs, C. N. Hunter, S. P. Armes and G. J. Leggett, *Chem. Sci.*, 2017, **8**, 4517-4526.
30. J. Madsen, R. E. Ducker, O. Al Jaf, M. L. Cartron, A. M. Alswieleh, C. H. Smith, C. N. Hunter, S. P. Armes and G. J. Leggett, *Chem. Sci.*, 2018, **9**, 2238-2251.
31. E. L. Elson and D. Magde, *Biopolymers*, 1974, **13**, 1-27.
32. K. Koynov and H.-J. Butt, *Curr. Opin. Colloid Interface Sci.*, 2012, **17**, 377-387.
33. O. Krichevsky and G. Bonnet, *Rep. Prog. Phys.*, 2002, **65**, 251-297.
34. C. Lellig, J. Wagner, R. Hempelmann, S. Keller, D. Lumma and W. Härtl, *J. Chem. Phys.*, 2004, **121**, 7022-7029.
35. U. Zettl, S. T. Hoffmann, F. Koberling, G. Krausch, J. Enderlein, L. Harnau and M. Ballauff, *Macromolecules*, 2009, **42**, 9537-9547.
36. P. Schwille, *Cell Biochem. Biophys.*, 2001, **34**, 383-408.
37. Y. Tian, M. M. Martinez and D. Pappas, *Appl. Spectrosc.*, 2010, **65**, 115A-124A.
38. S. A. Sukhishvili, Y. Chen, J. D. Müller, E. Gratton, K. S. Schweizer and S. Granick, *Nature*, 2000, **406**, 146.
39. J. Zhao and S. Granick, *J. Am. Chem. Soc.*, 2004, **126**, 6242-6243.
40. P. N. Sen, *J. Chem. Phys.*, 2003, **119**, 9871-9876.
41. T. K. Piskorz and A. Ochab-Marcinek, *J. Phys. Chem. B*, 2014, **118**, 4906-4912.
42. D. S. Novikov, E. Fieremans, J. H. Jensen and J. A. Helpern, *Nature Phys.*, 2011, **7**, 508-514.
43. M. Kac, *Am. Math. Mon.*, 1966, **73**, 1-23.
44. P.-F. Lenne, L. Wawrezinieck, F. Conchonaud, O. Wurtz, A. Boned, X.-J. Guo, H. Rigneault, H.-T. He and D. Marguet, *EMBO J.*, 2006, **25**, 3245-3256.
45. L. Wawrezinieck, H. Rigneault, D. Marguet and P.-F. Lenne, *Biophys. J.*, 2005, **89**, 4029-4042.
46. P. Asuri, S. S. Karajanagi, R. S. Kane and J. S. Dordick, *Small*, 2007, **3**, 50-53.
47. R. S. Kane, P. Deschatelets and G. M. Whitesides, *Langmuir*, 2003, **19**, 2388-2391.
48. N. Wisniewski and M. Reichert, *Colloids Surf. B*, 2000, **18**, 197-219.
49. D. Cunliffe, C. A. Smart, C. Alexander and E. N. Vulfson, *Appl. Environ. Microbiol.*, 1999, **65**, 4995-5002.
50. A. R. Hall and M. Geoghegan, *Rep. Prog. Phys.*, 2018, **81**, 036601.
51. A. Hucknall, S. Rangarajan and A. Chilkoti, *Adv. Mater.*, 2009, **21**, 2441-2446.
52. A. Roosjen, H. C. van der Mei, H. J. Busscher and W. Norde, *Langmuir*, 2004, **20**, 10949-10955.
53. S. A. Alang Ahmad, L. S. Wong, E. ul-Haq, J. K. Hobbs, G. J. Leggett and J. Micklefield, *J. Am. Chem. Soc.*, 2009, **131**, 1513-1522.
54. D. M. Jones, A. A. Brown and W. T. S. Huck, *Langmuir*, 2002, **18**, 1265-1269.
55. C. T. Culbertson, S. C. Jacobson and J. M. Ramsey, *Talanta*, 2002, **56**, 365-373.
56. P.-O. Gendron, F. Avaltroni and K. J. Wilkinson, *J. Fluorescence*, 2008, **18**, 1093-1101.
57. R. A. Erb, *J. Phys. Chem.*, 1968, **72**, 2412-2417.
58. M. E. Abdelsalam, P. N. Bartlett, T. Kelf and J. Baumberg, *Langmuir*, 2005, **21**, 1753-1757.
59. L. F. Mottram, S. Forbes, B. D. Ackley and B. R. Peterson, *Beilstein J. Org. Chem.*, 2012, **8**, 2156-2165.
60. L. Weger, M. Weidmann, W. Ali, M. Hildebrandt, J. S. Gutmann and K. Hoffmann-Jacobsen, *Langmuir*, 2018, **34**, 7021-7027.
61. C. Reznik and C. F. Landes, *Acc. Chem. Res.*, 2012, **45**, 1927-1935.
62. K. Åhlén, P. Ring, B. Tomasini-Johansson, K. Holmqvist, K.-E. Magnusson and K. Rubin, *Biochem. Biophys. Res. Commun.*, 2004, **314**, 89-96.
63. D. Axelrod, P. Ravdin, D. E. Koppel, J. Scledssinhger, W. W. Webb, E. L. Elson and T. R. Podleski, *Proc. Natl Acad. Sci. USA*, 1976, **73**, 4594-4598.
64. C. Dietrich, Z. N. Volovyk, M. Levi, N. L. Thompson and K. Jacobson, *Proc. Natl Acad. Sci. USA*, 2001, **98**, 10642-10647.
65. E.-M. Erb, K. Tangemann, B. Bohrmann, B. Müller and J. Engel, *Biochemistry*, 1997, **36**, 7395-7402.
66. D. E. Golan, C. S. Brown, C. M. L. Cianci, S. T. Furlong and J. P. Caulfield, *J. Cell Biol.*, 1986, **103**, 819-828.
67. H. G. Kapitza, D. A. Rüppel, H.-J. Galla and E. Sackmann, *Biophys. J.*, 1984, **45**, 577-587.
68. E. D. Sheets, G. M. Lee, R. Simson and K. Jacobson, *Biochemistry*, 1997, **36**, 12449-12458.
69. W. L. C. Vaz, M. Criado, V. M. C. Madeira, G. Schoellmann and T. M. Jovin, *Biochemistry*, 1982, **21**, 5608-5612.
70. W. L. C. Vaz, H. G. Kapitza, J. Stumpel, E. Sackmann and T. M. Jovin, *Biochemistry*, 1981, **20**, 1392-1396.
71. O. Hegener, L. Prenner, F. Runkel, S. L. Baader, J. Kappler and H. Häberlein, *Biochemistry*, 2004, **43**, 6190-6199.
72. S. Nelson, R. D. Horvat, J. Malvey, D. A. Roess, B. G. Barisas and C. M. Clay, *Endocrinology*, 1999, **140**, 950-957.
73. D. A. Roess, R. D. Horvat, H. Munnelly and B. G. Barisas, *Endocrinology*, 2000, **141**, 4518-4523.

